Build Simul (2021) 14: 1127–1146
https://doi.org/10.1007/s12273-020-0713-3

Fluid dynamic and thermal comfort analysis in an actual operating room with unidirectional airflow system

Nicola Massarotti[1], Alessandro Mauro[1] (✉), Salahudeen Mohamed[1], Andrzej J. Nowak[2], Domenico Sainas[1]

1. Dipartimento di Ingegneria, Università degli Studi di Napoli "Parthenope", Centro Direzionale, Isola C4, 80143 Napoli, Italy
2. Institute of Thermal Technology, Silesian University of Technology, Konarskiego 22, 44-100 Gliwice, Poland

Abstract

Air velocity and temperature distributions inside operating rooms (ORs) play a crucial role to reduce the risk of infections and to ensure adequate comfort conditions for patient and medical staff. In this work, the authors have developed a three-dimensional thermo-fluid dynamic model to simulate airflow and thermal comfort in an actual OR equipped with High-Efficiency Particulate Air (HEPA) filters. The model takes into account the presence of surgical lights, people and equipment within the room. An experimental campaign is carried out inside the actual OR to measure velocity and temperature, to be employed as boundary conditions for the numerical model. The experimental data have also been used to validate the numerical results. The validated model has been used to analyze the effects of human shape, thermal boundary conditions and buoyancy forces on the main thermal and fluid dynamic quantities in the OR. The thermal comfort is evaluated based on Predicted Mean Vote (PMV) and Predicted Percentage of Dissatisfied (PPD) indices. The results prove that the present experimental-numerical approach is useful to analyze and improve the thermal comfort conditions for medical staff and patient.

Keywords

heat and mass transfer,
thermal comfort,
operating room,
LAF system,
human body,
validation

Article History

Received: 18 May 2020
Revised: 03 August 2020
Accepted: 17 August 2020

1 Introduction

Operating rooms (ORs) represent the environment inside healthcare buildings that require the greatest deal of attention in terms of heating, ventilation and air conditioning (HVAC) systems, in order to reduce the risk of infection for patients and medical staff, and to maintain adequate thermo-hygrometric conditions to ensure comfort (Chow and Yang 2003). HVAC systems are generally designed on the basis of technical standards and common practice, with most of recent advancements being tested in experimental set-up chambers or lab controlled environments (ISO14644-1 2015; ISO14644-2 2015; DIN-1946-4 2016).

The choice of the ventilation system is very important, in fact, Surgical Site Infections (SSIs) occur in 2.9% of all surgical operations, carried out conventionally in ORs, as estimated by Knobben et al. (2006). Nobile et al. (2015) reported that in orthopaedic and trauma surgery patients, SSI is associated with additional medical costs of €32000, related to uninfected patients, corresponding to an average cost per SSI of €9560. Therefore, horizontal and vertical unidirectional flow (UDF) ventilation systems have been studied in the recent years, due to the importance of clean air circulation inside ORs (Chow and Yang 2004; Loomans et al. 2008; Zoon et al. 2011).

An appropriate ventilation system is essential for air quality, and to dilute and remove airborne bacteria from the surgical area. It must also provide comfortable working conditions and appropriate levels of thermal comfort for medical staff and patient during a surgery (van Gaever et al. 2014).

Nowadays, the most common ventilation systems used in ORs are based on laminar air flow (LAF) ventilation and mixing ventilation. With LAF ventilation, a large volume of air is provided with a uniform flow field over the surgical area. The aim of these ventilation systems is to remove microbiological contamination from the critical area and prevent bacteria-carrying particles (BCPs) from being deposited on wounded surfaces (Chow and Yang 2004). Indeed, LAF

E-mail: alessandro.mauro@uniparthenope.it

List of symbols

c_p	specific heat (J/(g·K))
f_{cl}	surface area factor of clothing
g	gravity (m/s^2)
h_c	convective heat transfer coefficient (W/(m^2·°C))
I_{cl}	clothing insulation (m^2·°C/W)
k	thermal conductivity (W/(m·K))
M	metabolic rate (W/m^2)
p	pressure (Pa)
p_a	water vapour partial pressure (Pa)
t	time
t_a	air temperature (°C)
t_{cl}	clothing surface temperature (°C)
$\overline{t}_r$	mean radiant temperature (°C)
T	temperature (°C)
U	velocity (m/s)
v_{ar}	relative air velocity (m/s)
W	mechanical work done (W/m^2)
β	thermal expansion coefficient (°C^{-1})
μ_T	turbulent viscosity (Pa·s)
μ	laminar viscosity (Pa·s)
ρ	density (kg/m^3)

Acronyms

BC	boundary condition
Case A	human body shape
Case B	cylindrical shape
HEPA	high-efficiency particulate air
HVAC	heating, ventilation and air conditioning
LAF	laminar air flow
OR	operating room
PMV	predicted mean vote
PPD	predicted percentage of dissatisfied
SZ	sterile zone

systems are being adopted in ORs for two main reasons: energy saving and reduction of infection risk. Lewis et al. (1969) showed that under LAF conditions, transfers of bacterial aerosol to the area above the operation table can be considerably reduced. Friberg and Friberg (2005) evaluated two types of ultra-clean LAF ventilation concepts, and they conclude that both down-flow and lateral-flow ventilation systems are equally efficient in terms of airborne bacteria reduction at wound site.

Brohus et al. (2008) analysed two disturbances in an OR: door opening during an operation and the activity level of medical staff. A similar activity was carried out by Sadrizadeh et al. (2018), who analysed air quality and level of airborne particles during single and multiple door-opening cycles.

A number of researches studied unidirectional airflow systems within chambers reproduced in laboratory environments, by using PIV technique (McNeill et al. 2013), while others compared numerical results with PIV data (Jeter and Stevenson 2013). Balocco et al. (2015) compared the numerical investigation and experimental results on the airflow pattern and thermal field in a real OR. Romano et al. (2015) showed that CFD modelling is an important tool to simulate the performance of actual ORs in terms of airborne particle contamination control, thermal field and airflow pattern.

The position of surgical light and space availability for the medical staff, medical equipment and surgical table can negatively affect the performance of this type of ventilation system (Zoon et al. 2010). It was shown that thermal comfort conditions for the medical staff can be compromised based on the chosen system solution (van Gaever et al. 2014), as this can easily affect the unidirectional airflow pattern of a vertical LAF system (Chow et al. 2006; Méndez et al. 2008). Slight modifications of the geometry can bring great improvements in the efficiency of the air ventilation flow, though, some disadvantages due to the unidirectional airflow still remain (Méndez et al. 2008). To avoid disadvantages of vertical airflow systems, horizontal LAF has been suggested as an alternative (Ahl et al. 1995; Liu et al. 2009), even if this ventilation system is very sensitive to the internal locations of medical staff and equipment in the OR. Chow and Yang (2004) and Chow et al. (2006) proposed an investigation of the combined effect of surgical lights and air discharge velocity on indoor ventilation performance. A comprehensive experimental and numerical analysis was proposed by Kameel and Khalil (2003), concerning airflow and heat transfer inside an OR, taking into account medical staff, surgical table, medical equipment and surgical lights.

In a previous study of the authors of this paper (Massarotti et al. 2019), an experimental campaign in an actual OR, equipped with ceiling swirl diffusers, was carried out to measure airflow distribution near the surgical site and to validate the numerical model. Those results proved that the experimentally obtained data are essential to define appropriate boundary conditions in the numerical model and to reproduce the actual flow conditions inside ORs (Massarotti et al. 2019).

As concerns the activities related to heat transfer on humans, there are numerous studies regarding natural convection heat transfer coefficient in adults, based on

direct measurements and thermal manikins (Mitchel et al. 1969; Clark and Toy 1975), as well as based on numerical simulations (Ginalski et al. 2007; Najjaran 2012). Ostrowski et al. (2016) and Ostrowski and Rojczyk (2018) assessed the body dry heat loss from an infant in radiant warmer, copper cast anthropomorphic thermal manikin and controlled climate chamber laboratory setup.

In addition, in the literature, the influence of the manikin shape on indoor airflow was analysed (Topp et al. 2002, 2003; Zukowska et al. 2007), by investigating the influence of geometry of the actual manikin on air distribution, convective heat transfer and particle concentration. In order to investigate the local conditions that affect thermal comfort of medical staff and patients, detailed geometries must be considered.

The evaluation of thermal comfort of the occupants of hospitals and health care units is important to understand both the post-operative complications in patients and the thermal sensation of the medical staff and patient during surgical activity, in order to employ this information to rectify the current problems faced by the medical community. Several studies were carried out in assessing the thermal comfort in hospitals by considering different factors, such as design of the HVAC systems, position of the occupants and equipment. Verheyen et al. (2011) performed a thermal comfort study by means of questionnaires results and thermal comfort indices, i.e. predicted mean vote (PMV) and predicted percentage of dissatisfied (PPD) indices, were calculated to predict the thermal sensation of the hospital wards. In the study of Pourshaghaghy and Omidvari (2012), a thermal comfort study was carried out in hospital, using experimental measurements for understanding the performance of HVAC systems and the consequent thermal comfort level. The study showed that the thermal indices computed from the experimental measurements were not within the ISO standards. A numerical study was performed by Ho et al. (2009) in a hospital surgery room, for evaluating the thermal comfort indices and the results elucidated the fact that by improving the design of HVAC systems, a better thermal sensation for the occupants can be achieved.

Numerical modelling have proven to be a reliable non-invasive tool in predicting the engineering quantities for improving design of ORs and for providing favourable indoor air conditions for the occupants, as corroborated in the above mentioned studies. Moreover, due to the difficulties involved in carrying out experimental measurements in ORs, numerical methods have to be properly calibrated and a standard numerical procedure concerning the flow and thermal boundary conditions for the OR walls, equipment, and occupants has to be defined, in order to obtain accurate results. Therefore, in this study, the authors have employed a numerical model that implements boundary conditions, for velocity and temperature values, deriving from the data measured in the current experimental analysis, for investigating the thermo-fluid dynamics in a real OR. Moreover, the numerical results obtained from the simulations are validated against the experimental data acquired in the OR, given the importance of employing validated models (ASME 2009; Arpino et al. 2013, 2015, 2016; Massarotti et al. 2016). Therefore, the experimentally validated numerical model is employed in this study to achieve two main objectives: (i) analyze the effects of different thermal boundary conditions, for two configurations of human geometries in a real OR under "at-rest" conditions, on the flow and thermal fields in a real OR; (ii) carry out a thermal comfort analysis, aimed at the calculation of PMV and PPD indices.

Thermal comfort is studied from the thermo-fluid dynamic numerical results, using Fanger's comfort model (ISO-7730). PMV and PPD indices have been calculated to analyse the thermal sensation inside the OR, due to different thermal boundary conditions at the surface of the human models employed in this study. In particular, a detailed study on flow and thermal fields at the sterile zone (region where patient and medical staff are positioned) is performed. The obtained results can be used as benchmarks for the future studies in selecting the appropriate thermal boundary conditions to predict proper engineering quantities in ORs.

The paper is structured as follows: the next section presents the case study of a real OR in a hospital near Napoli, in Southern Italy, the experimental set-up and the computational model. Section 3 describes the results obtained, while some conclusions are drawn in the last section.

2 Methods: experimental and numerical analysis

2.1 Case study

The authors carried out an experimental investigation in a real OR of a hospital near Napoli, in Southern Italy. The layout of the OR considered in this work is reported in Figure 1. The net height of the room is 2.8 m and its surface is 36.6 m^2. The OR is provided with unidirectional ventilation system composed of 6 HEPA H14 filters (4 with dimensions of 610 mm × 910 mm and 2 with dimensions of 610 mm × 610 mm) installed in a plenum of 2.4 m × 2.4 m, as shown in Figure 1.

The use of horizontal filters allows obtaining a uniform air distribution in the critical area above the surgical site. At each corner of the OR, two extraction grilles are installed. The ventilation system of the OR is designed to ensure ISO 5 class conditions. In order to respect these limitations in terms of air quality and contamination control, 3200 m^3/h of air (corresponding to 30 air changes per hour—ACH) are injected from the ceiling filters. The HVAC system is

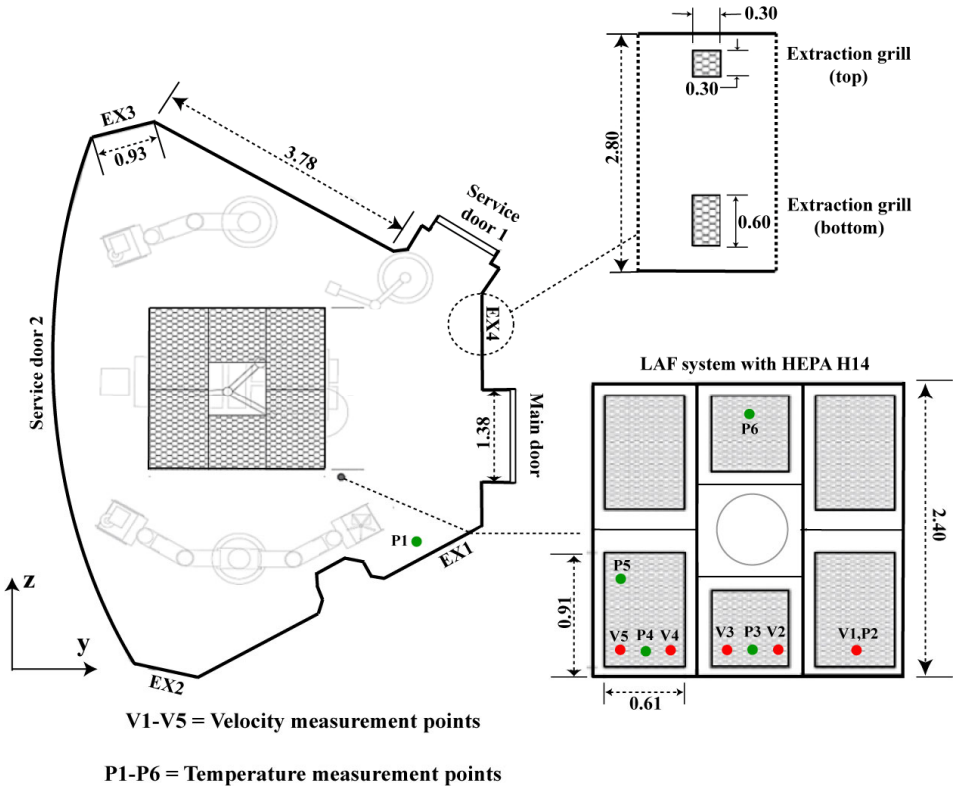

Fig. 1 Layout of the OR (dimension are in meters), velocity measurement points (V_i) and temperature measurement points (P_i) at 2.2 m height, under the ceiling filters

controlled through a variable volumetric flow (VAV) damper actuator. However, in order to verify the air volumetric flow rate injected inside the room, the authors have connected the adjustment device (ZTH EU, Belimo) on the actuator. This device communicates with the controller using the voltage signal line for the actual value or set-point value. This instrument allows accessing the available operating values and parameters.

In order to avoid the risk of contaminant infiltrations from adjacent environments, an overpressure of +15Pa (set-point value) is maintained in the OR by extracting 90% of air flow rate that enters the room. Air is supplied through the ceiling filters at a design set-point temperature of 23 °C and 50% relative humidity.

A three-dimensional computational domain of the actual room has been reconstructed, taking into account the actual dimensions of the OR under investigation, and it is reported in the section dedicated to the computational model.

2.2 Experimental set-up

During the experimental campaign, the HVAC system supplied a constant air flow rate at a specific set point temperature (°C) and relative humidity (%). Microclimate measurements were carried out in "*at-rest*" conditions (room fully equipped with services and instruments, but without medical staff and patient). The experimental campaign has been carried out over a day, from 8:00 a.m. to 15:00 p.m., keeping all doors closed. For microclimate measurements, the authors have used hot-wire anemometer, NTC air-temperature and humidity sensor (connected to a multifunction meter Testo 435-2), thermocouples (type K) and IR Camera (FLIR S40). All instruments have been calibrated before the experimental campaign.

The technical specifications of the Testo instruments used during the experimental campaign are reported in Table 1.

Table 1 Technical specifications of the probes (connected to a Testo 435-2)

Instrument	Temperature range (°C)	Velocity range (m/s)	Relative humidity range	Accuracy
Hot wire anemometer (ϕ7.5mm)	—	0 to 20	—	±(0.03 m/s + 5% m.v.)
NTC	−20 to +70	—	—	±0.3 °C
Hygrometer	—	—	0 to 100%	±2% (+2% to 98%)

All microclimate instruments were connected to a data logger, which provides the average values of the parameters measured over a 60 seconds acquisition time (average, maximum and minimum values). As regards the air velocity and temperature measurements, the analysis has been carried out at different points of the room (V1–V5 for velocity measurements, P1–P6 for temperature measurements), as illustrated in Figure 1.

As regards temperature measurements, the authors have also analysed the surface temperature on the glass and on the back of the surgical lights, by means of a type K thermocouple placed on several points of the surgical light. The type K thermocouple was used in order to determine the surface temperature to be used as boundary condition in the numerical model.

2.3 Computational model

The governing equations implemented in the present steady-state model to reproduce the velocity and temperature fields of air inside the OR are represented by the continuity and Navier-Stokes equations for an incompressible fluid and by the energy conservation equation, as follows (Nithiarasu et al. 2007):

Mass conservation equation:

$$\nabla \cdot U = 0 \tag{1}$$

Momentum conservation equation:

$$\rho \nabla \cdot (UU) = \nabla \cdot ((\mu + \mu_T)\nabla U) - \nabla p + \rho g \beta \Delta T \tag{2}$$

Energy conservation equation:

$$\rho c_p U \cdot \nabla T = k \nabla^2 T \tag{3}$$

where ρ is the fluid density, U (u, v, w) is the Reynolds averaged velocity vector, p is the pressure, μ is the fluid viscosity, μ_T is the turbulent viscosity, g is the gravity, k stands for the thermal conductivity, c_p is the isobaric specific heat and β is the thermal expansion coefficient of air. Boussinesq approximation is used to model the buoyancy effects by relating the density difference to the thermal gradients inside the operating room. Fluid properties have been referred to dry air, since the difference with the values corresponding to humid air can be considered negligible.

The thermal comfort level inside the OR is evaluated by means of Fanger's comfort equation (ISO-7730 2006). The thermal comfort indices, i.e. PMV and PPD, are based on the thermal balance of human body. PMV represents the mean value of the votes of a large group of persons on the seven points thermal sensation scale as shown in Table 2.

Table 2 Seven point thermal sensation scale

PMV	Thermal sensation
+3	Hot
+2	Warm
+1	Slightly warm
0	Neutral
−1	Slightly cool
−2	Cool
−3	Cold

PPD is an index which establishes a quantitative prediction of percentage of thermally dissatisfied persons among a group of people. These indices are calculated as follows:

$$\begin{aligned}\mathrm{PMV} = {} & (0.303\mathrm{e}^{-0.036M} + 0.028)\{(M-W) - 3.05\times10^{-3} \\ & \times[5733 - 6.99(M-W) - p_a] - 0.42\times[(M-W) - 58.15] \\ & - 1.7\times10^{-5} M(5867 - p_a) 0.0014M(34 - t_a) - 3.96\times10^{-8} f_{cl} \\ & \times[(t_{cl}+273)^4 - (\bar{t}_r + 273)^4] - f_{cl} h_c (t_{cl} - t_a)\}\end{aligned} \tag{4}$$

where

$$\begin{aligned}t_{cl} = {} & 35.7 - 0.28(M-W) - I_{cl}\{3.96\times10^8 f_{cl} \times \\ & [(t_{cl}+273)^4 - (\bar{t}_r + 273)^4] + f_{cl} h_c (t_{cl} - t_a)\}\end{aligned} \tag{5}$$

$$h_c = \begin{cases} 2.38(t_{cl} - t_a)^{0.25} \\ 12.2\sqrt{v_{ar}} \end{cases} \quad \text{for} \quad \begin{cases} 2.38(t_{cl} - t_a)^{0.25} > 12.1\sqrt{v_{ar}} \\ 2.38(t_{cl} - t_a)^{0.25} < 12.1\sqrt{v_{ar}} \end{cases} \tag{6}$$

$$f_{cl} = \begin{cases} 1.00 + 1.290 I_{cl} \\ 1.05 + 0.645 I_{cl} \end{cases} \quad \text{for} \quad \begin{cases} I_{cl} \le 0.078\ (\mathrm{m}^2 \cdot {}^{\circ}\mathrm{C/W}) \\ I_{cl} > 0.078\ (\mathrm{m}^2 \cdot {}^{\circ}\mathrm{C/W}) \end{cases} \tag{7}$$

where
M is the metabolic rate (W/m²);
W is the mechanical work done (W/m²);
I_{cl} is the clothing insulation (m²·°C/W);
f_{cl} is the surface area factor of clothing;
t_a is the air temperature (°C);
$\bar{t}_r$ is the mean radiant temperature (°C);
v_{ar} is the relative air velocity (m/s);
p_a is the water vapour partial pressure (Pa);
h_c is the convective heat transfer coefficient (W/(m²·°C));
t_{cl} is the clothing surface temperature (°C).

$$\mathrm{PPD} = 100 - 95\times \mathrm{e}^{-(0.03353\times \mathrm{PMV}^4 + 0.2179\times \mathrm{PMV}^2)} \tag{8}$$

However, it should be noted that healthcare workers' mask and gown wearing can decrease the neutral temperature significantly.

A 3D computational domain of the actual OR has been reconstructed and different geometries for the medical staff and patient have been considered in this work, as shown in Figure 2.

In particular, two cases have been taken into account: medical staff and patient modelled with a detailed human body shape of height 1.70 m and surface area of 1.8 m^2 (Case A) (Fojtlín et al. 2018), and with cylindrical shape having the same height and the same external surface area (Case B).

2.4 Boundary conditions

The boundary conditions implemented in both computational domains of Case A and Case B (refer to Figure 2), together with the surface area of the inlet laminar diffusers and of the extraction grilles, are reported in Table 3. Air is used as working fluid and the values of the physical and thermal properties of air used in the numerical model are reported in Balocco et al. (2014). The employed boundary conditions have been determined during the experimental campaign, and are reported in Tables 4 and 5. The inlet velocity has been obtained by measuring the average velocity below the ceiling filters at a distance of 0.55m in different points. The temperature of the surgical light (surface glass and cover), monitor and medical electrical equipment have been measured by means of type K thermocouple.

Two different thermal boundary conditions, i.e. constant temperature and constant heat flux, are assigned at the surface of medical staff and patient in order to study their influence on the thermal field distribution inside the OR. In particular, temperature values are imposed on the different surfaces of the human body, as reported in Table 4, for the real human shapes (Case A), while an average constant temperature of 36 °C is imposed on the cylindrical surface, for the cylinder shape (Case B). The alternative boundary conditions employed for medical staff and patient, reported in Table 5, consist in imposing a heat flux of 24.4 W/m^2 and 14.1 W/m^2 on medical staff and patient, respectively, for both Case A and Case B.

Since the skin temperature or heat flux are imposed on human body, human thermoregulation system is not relevant for this work, as heat transfer within the body of medical personnel or patient is not analysed.

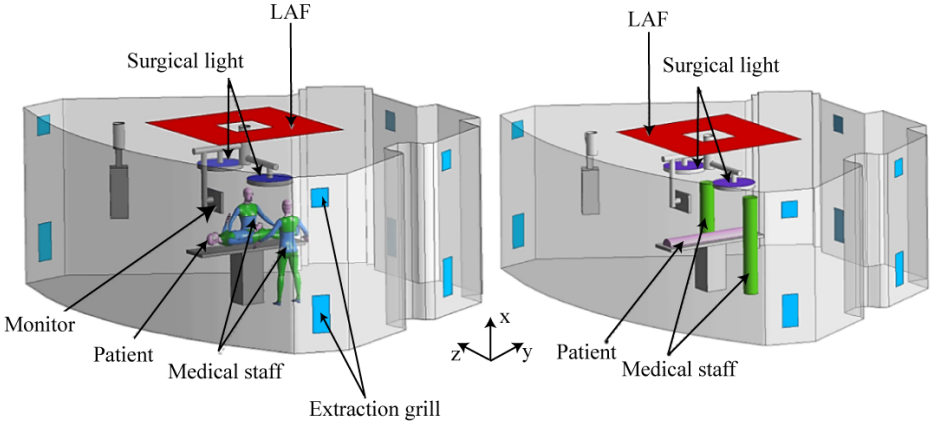

Fig. 2 Computational domain of OR with medical staff and patient for: Case A: human body shape (left) and Case B: cylindrical shape (right)

Table 3 Geometry details and boundary conditions

Objects	Surface area (m^2)	Boundary conditions
Inlet (LAF system)	5.76	Velocity inlet
Outlet (bottom grill)	0.18	Pressure outlet
Outlet (top grill)	0.09	
Walls	—	No slip velocity and wall functions
Surgical light	0.45×2	Temperature
Cover (surgical light)	0.45×2	
Medical staff and patient (Case A)	1.8	Temperature and heat flux
Medical staff and patient (Case B)	1.8	
Monitor	0.19	Heat flux

Table 4 Boundary conditions employed

Objects	Boundary conditions	Value	Source
Inlet	Velocity inlet	0.3 m/s	Measured
Outlet	Pressure outlet	0 Pa	Balocco et al. 2014, 2015; Sadrizadeh et al. 2014; Romano et al. 2015
Walls	No slip velocity and wall functions	—	—
Surgical light (glass)	Temperature	27.5°C	Measured
Surgical light (cover)		29.2°C	
Monitor	Heat flux	400 W/m^2	Wilkins and McGaffin 1994; McNeill et al. 2012
Head	Temperature	36.0 °C	Gordon et al. 1976; Fiala et al. 1999; Van Leeuwen et al. 2000; Diao et al. 2003; Laszczyk and Nowak 2016
Body		36.0 °C	
Neck		36.4 °C	
Leg		32.0 °C	
Foot		29.3 °C	
Chest		33.9 °C	
Thigh		32.9 °C	
Abdomen		33.2 °C	
Hand		29.9 °C	
Arm		32.9 °C	
Temperature (inlet)	Temperature	23.0 °C	Measured
Temperature (outlet)		23.0 °C	

Table 5 Alternative boundary conditions employed for medical staff and patient

Objects	Boundary conditions	Value	Source
Medical staff	Heat flux	24.4 W/m^2	Wilkins and McGaffin 1994; McNeill et al. 2012; Romano et al. 2015
Patient		14.1 W/m^2	

2.5 Numerical methodology

The numerical model is based on Reynolds Averaged Navier-Stokes (RANS) approach. Numerical simulations are performed in the buoyantBoussinesqSimpleFoam solver in OpenFOAM 4.0. The authors have used the realizable k-ε turbulence model (Shih et al. 1995), which has already proven to be appropriate for calculating airflow and heat transfer phenomena in complex ventilated indoor environments (Massarotti et al. 2019). Moreover, radiation effects have been not considered in this study. Turbulence intensity of 5% at the inlet section has been employed (Balocco et al. 2014, 2015; Romano et al. 2015). The discretization of turbulent kinetic energy and turbulent dissipation, such as the advection terms, has been carried out with second-order upwind scheme, and wall-functions have been employed. The choice of the turbulence closure model for calculation of airflow in ventilated spaces and design of HVAC systems should take into account both accuracy and computing resources.

PMV and PPD indices are calculated in an ad hoc code developed in OpenFOAM, based on the flow and thermal fields obtained from the simulations.

3 Results and discussion

3.1 Grid sensitivity analysis

The computational domain has been discretized with an unstructured mesh of tetrahedral elements, as shown in Figure 3. A mesh sensitivity analysis, based on three different grids, has been carried out in order to obtain grid independent results and optimize computational time. The results are reported in Figure 4, in terms of velocity and temperature at plane height of 1.5 m.

In Figure 4, the results obtained with grid 1 (5,946,921 tetrahedral elements) and grid 2 (10,739,463 tetrahedral elements), in terms of velocity magnitude and temperature values, calculated on the midline at plane height of 1.5 m, have been compared with the results obtained for the same quantities with grid 3 (14,627,162 tetrahedral elements), considered as reference. In particular, the meshes are refined

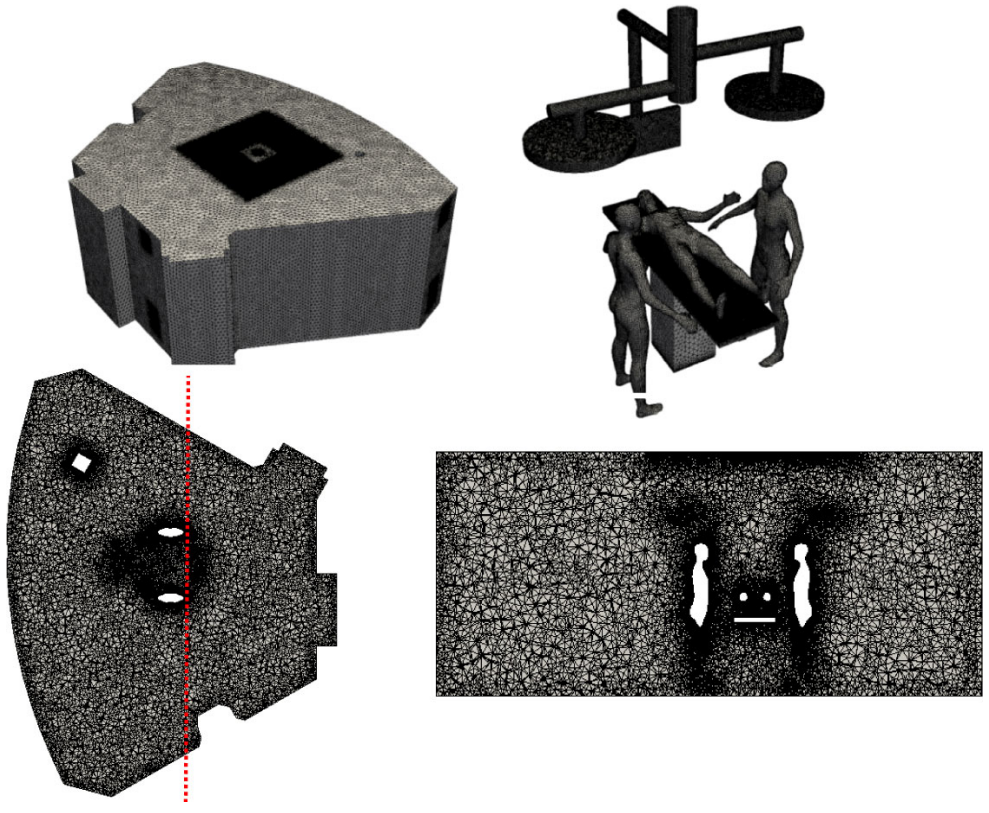

Fig. 3 Computational grid of the OR with real human shapes and other equipment

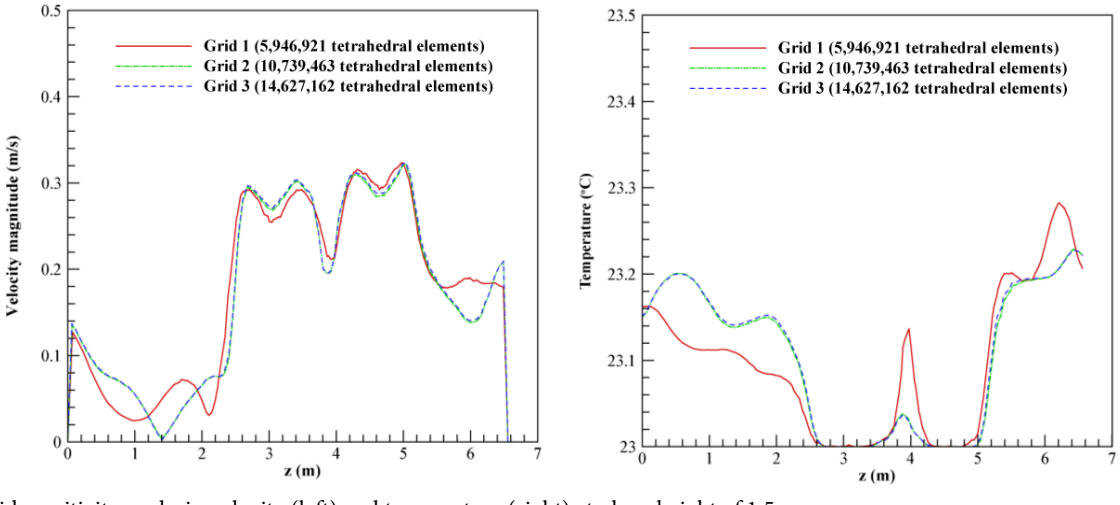

Fig. 4 Grid sensitivity analysis: velocity (left) and temperature (right) at plane height of 1.5 m

in the regions where gradients of the physical quantities are larger, such as near air supply, air extraction, medical staff, patient and surgical light. The selected mesh, shown in Figure 3, is the grid 2 (10,739,463 tetrahedral elements), since the relative difference, on velocity and temperature, with respect to the third mesh is smaller than 1.0%.

3.2 Validation of the numerical model

The numerical model developed in this work has been validated against the experimental data acquired on-site inside the OR. For this purpose, the numerical simulations have been performed without incorporating the human shape models, for two different cases, i.e. with and without the buoyancy effects. The comparison of the numerical results with the experimental data are reported in Figure 5, in terms of air velocity on a line at 2.2 m height under the ceiling filters (refer to Figure 1, points V1–V5).

The measured values are reported both in terms of average velocity velocity and expanded combined uncer-

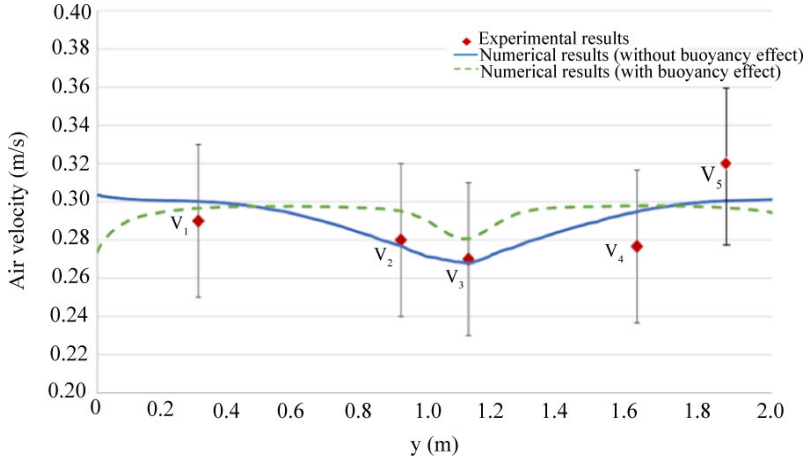

Fig. 5 Comparison between experimental and numerical results at 2.2 m height under the ceiling filters

tainties, calculated combining type A and type B uncertainties and by using a coverage factor $k = 1$, corresponding to a 68% confidence level (Arpino et al. 2011). From the analysis of Figure 5, it can be noticed that the numerical results obtained both considering and neglecting the buoyancy effects are in excellent agreement with the experimental data. The difference between the results obtained in presence and in absence of buoyancy effects is not significant (smaller than the experimental uncertainty), since forced convection plays an important role on the convection inside the room. The maximum difference between the numerical results and the experimental data is approximately equal to 6.6%, and this value is smaller than the minimum measurement uncertainty value, equal to 8.7%. Moreover, Table 6 reports the comparison between the experimental and numerical results in terms of temperature values at six different points inside the OR (P1–P6). And a good agreement is observed.

Table 6 Comparison of experimental and numerical results in terms of temperature values at point P1–P6 (refer to Figure 1)

Measurement points	Height (m)	Numerical results (°C)	Experimental results (°C)
P1	0.45	23.1	23.2
P2	2.20	23.2	23.0
P3		23.2	23.1
P4		23.1	22.7
P5		23.0	22.7
P6	1.94	22.9	22.4

3.3 Velocity evaluation

After the validation of the numerical model against the experimental data measured in the present work, numerical simulations have been carried out for two different geometries of the occupants inside the OR: Case A, in which the occupants are modelled in detail in terms of their real human body shape; Case B, in which the people in the room are modelled as cylinders. In each case, two different thermal boundary conditions, i.e. constant temperature and constant heat flux boundary conditions are assigned on the people surfaces, in order to analyse velocity and temperature fields inside the OR. In particular, the boundary conditions assigned at the OR computational domain are obtained from the velocity and temperature values measured in the experimental analysis (refer to Table 4). It is important to keep in mind that according to Boussinesq approximation for buoyancy effects, the density difference of air is due to the thermal gradients in the OR, which consequently influences the fluid flow. Since the current study is focused on the effects of different thermal boundary conditions on the human models, the buoyancy effects have an important role in the fluid flow, particularly at the sterile zone, where the occupants are positioned. Therefore, the numerical studies are carried out taking into account the buoyancy effects, by considering gravity in the downward 'x' direction, for the two different thermal boundary conditions assigned on humans. Moreover, the velocity, temperature and thermal indices profiles obtained with buoyancy effects cases are compared against the corresponding without buoyancy effect cases.

Figure 6 shows the results obtained in terms of air velocity contours and path lines inside OR, for a constant temperature boundary condition imposed on the people surfaces with human shape (Case A) in the presence of buoyancy. The air from the inlet diffuser enters the OR at a velocity of 0.3 m/s and encounters surgical lights and table, equipment, staff and patients, with consequent recirculation regions outside the sterile area.

The ceiling air diffuser can ensure a unidirectional airflow over the surgical table, with a consequent flushing of the critical area as shown in Figure 6(b). The discharge

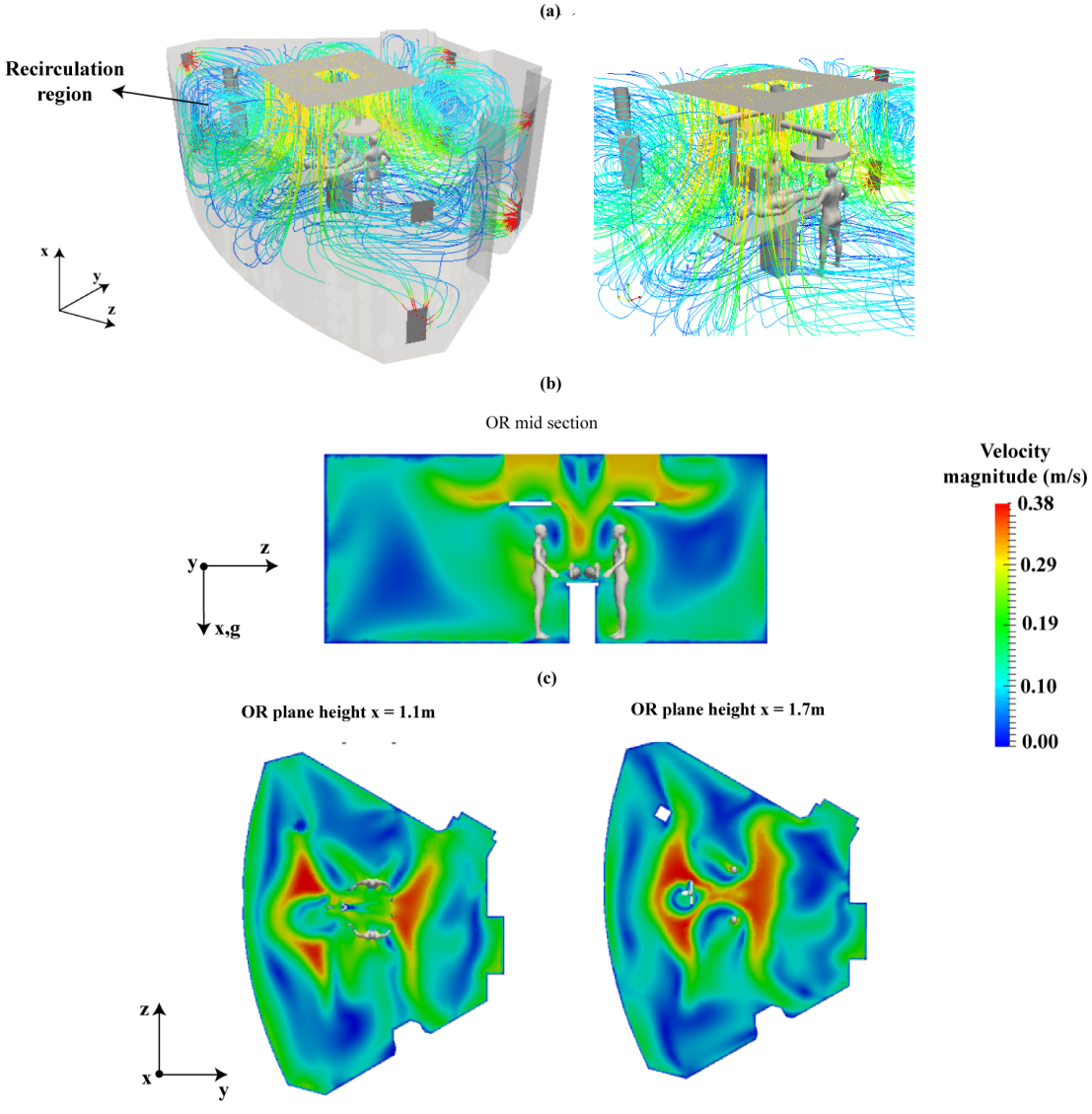

Fig. 6 Constant temperature boundary condition on people surfaces, for Case A (real human body shape) with buoyancy effects: (a) velocity path lines and contours; (b) velocity contours at OR mid-section; (c) velocity contours at two OR plane heights

airflow from the unidirectional diffuser accelerates as it approaches the surgical table, due to the presence of surgical lights. In particular, the air flow through the surgical lights undergoes diversion at a velocity around 0.38 m/s. It can be noticed that the resultant air flow direction between the two surgical lights passes through the staff mainly near face, chest and abdomen at a velocity below 0.25 m/s. It can be observed that there are areas of low-velocity recirculation, both under the surgical lights and close to the walls of the OR, where no extraction grilles are installed. Moreover, due to recirculation regions, the air from the non-sterile zones (regions away from the medical staff) may carry contaminants, which can interact with the sterile zone (area containing patient and medical staff), thus causing higher chances of surgical site infection. Figure 6(c) reports the velocity field on two horizontal planes at 1.1 m (typical surgical table height) and 1.7 m heights (typical human head-neck height), for constant temperature boundary conditions. At 1.1 m height, the air velocity near the patient assumes values below 0.15 m/s. In particular, the present air velocity values close to the patient's area can be considered acceptable during surgery, as suggested in reference (Memarzadeh and Manning 2002). In fact, the air velocity near the wound site should not exceed 0.2 m/s to prevent excessive drying (Al-Waked 2010). The Standard 170-2017 (ANSI/ASHRAE/Standard-170) recommends a supply of unidirectional airflow downward over the surgical table and medical staff, which sufficiently covers the entire sterile zone, as in the present case. At 1.7 m height (Figure 6(c)), i.e. at the head and neck of the medical staff, velocity values are around 0.25–0.30 m/s. These larger velocities are due to the obstruction of the air flow caused by the surgical lights, which reduce the area for the airflow.

These velocities are slighlty larger than the suggested ones (lower than 0.2 m/s) and could be related to slight discomfort conditions during long surgeries, if occurring in the physical reality. However, it should be pointed out that these values depend on many factors, such as the position of people, lamps, monitors and equipment and, therefore, can be optimized.

There is a significant influence on the airflow inside the OR, as shown in Figure 6(c), due to the mutual dependance of air velocity and temperature distribution. The imposition of heat flux at monitor and temperature boundary conditions at the medical staff and patient induce higher temperature gradients and, therefore, larger air velocites are observed at the sterile zone, with respect to non-sterile zones, particularly at plane hights of 1.1 m and 1.7 m. The air velocities prediced at the sterile zone are within acceptable range, i.e. ~ 0.08–0.2 m/s, particularly in the zone near the patient.

Figure 7 depicts the velocity profiles plotted at the sterile

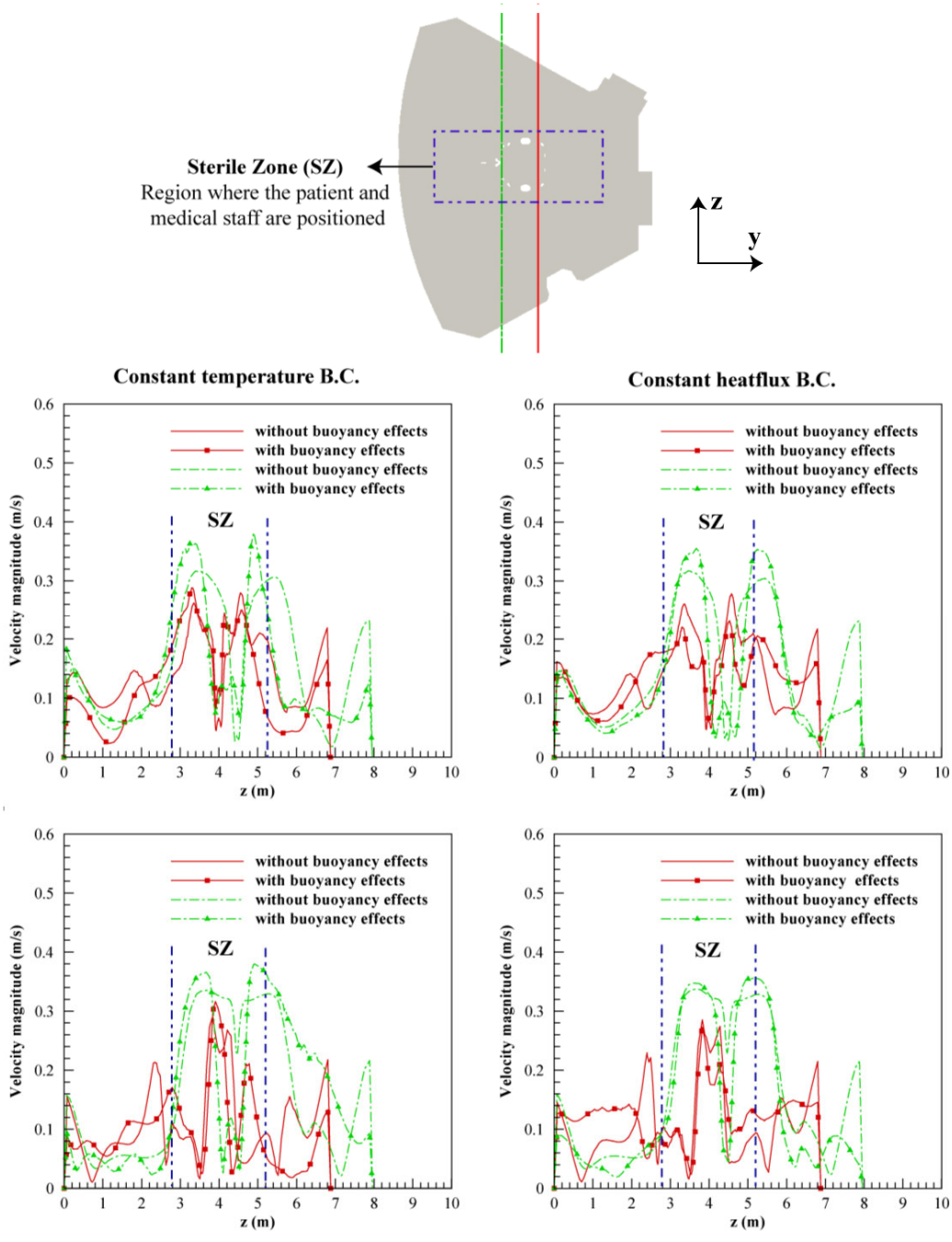

Fig. 7 Velocity profiles at two sections of the OR (green and red lines), at plane heights of 1.1 m (top) and 1.7 m (bottom) for human body shape (Case A), obtained imposing temperature (left) and heat flux (right) boundary conditions on the human bodies (refer to Tables 4 and 5 for the values)

zone (SZ) in the OR for two different thermal boundary conditions imposed on people surfaces, i.e. temperature and heat flux (refer to Tables 4 and 5 for the values), reproduced with real human body (Case A). In the case of constant heat flux boundary condition assigned at the real human models, the air velocity values inside the OR are the same of those obtained for constant temperature boundary condition, if buoyancy effects are neglected. Instead, if the buoyancy effects are taken into account, air velocity values are influenced by the kind of thermal boundary condition on people surfaces. In particular, if temperature is imposed on the human bodies, the maximum values of the calculated velocities can be up to 20% larger than those calculated by imposing heat flux, proving the importance of thermal boundary conditions on the results. Moreover, the buoyancy effects should be considered in the model, since they influence the air flow pathlines and velocities, and a difference of 15% is calculated on the maximum velocity values with respect to the case in the absence of buoyancy effects.

In order to consider the effects of simplified geometry for people inside the OR, commonly used in the literature, cylindrical shape (Case B) is also taken into account to represent medical staff and patient. The velocity contours and velocity profiles are reported, respectively, in Figure 8 and Figure 9, for two different thermal boundary conditions on the cylinders, i.e. constant temperature and constant heat flux (refer to Tables 4 and 5 for the values). Larger velocities are appreciated in presence of temperature boundary conditions. From the analysis of Figure 9, the velocity values calculated in presence of cylinders (Case B) at plane heights of 1.1 m and 1.7 m can differ of about 15% with respect to the values calculated for the case of real human shape (Case A), proving the importance of considering realistic shape for medical staff and patient.

3.4 Temperature evaluation

Figure 10 depicts the temperature contours obtained for the real human body shape (Case A) with two thermal boundary conditions on people surfaces, i.e. temperature and heat flux (refer to Tables 4 and 5 for the values), in presence of buoyancy effects. It is interesting to note that, due to the large Air Change per Hour (ACH), there is a reduction of air temperature at the non-sterile zones. Instead, at the sterile area, where patient and medical staff are positioned, larger temperature gradients are observed, corroborating the fact that the thermal boundary conditions imposed on the human surfaces play an important role in determining the temperature distribution inside the OR.

The large air velocity between the surgical lights induces homogenous temperature of 23 °C, particularly in the area between medical staff and patient. In the constant temperature boundary condition case, the area around the head of medical staff is at a temperature of 24.7 °C, due to the surgical lights located just above the head, due to low velocity recirculation regions (Figure 10 left). Moreover, the air flow around the patient transports the heat towards the legs of the medical staff, thereby increasing the temperature levels. The scenario is quite different for constant heat flux boundary condition (Figure 10 right), since the temperature values at the sterile zone are lower, if compared to constant temperature boundary condition. Therefore, the imposition of thermal boundary conditions is important for the assessment of the temperature levels inside the OR.

Figure 11 depicts the temperature profiles plotted at two sections of the OR, at plane heights of 1.1 m and 1.7 m. As mentioned before, from Figure 11, it is evident that temperature values are larger in the case of constant temperature boundary condition, if compared to constant heat flux boundary condition, with a maximum difference around 6%. In particular, a maximum temperature of 26.3 °C (green line) is observed at the plane height of 1.1 m in Figure 11 (top) for a constant temperature boundary condition, without buoyancy effects. At this section, the head of the patient is located, and it is near the monitor, which has a heat flux of 400 W/m^2. Since the air velocity values are low (0.05–0.08 m/s), the temperature gradients are larger and, therefore, the head of the patient experiences an

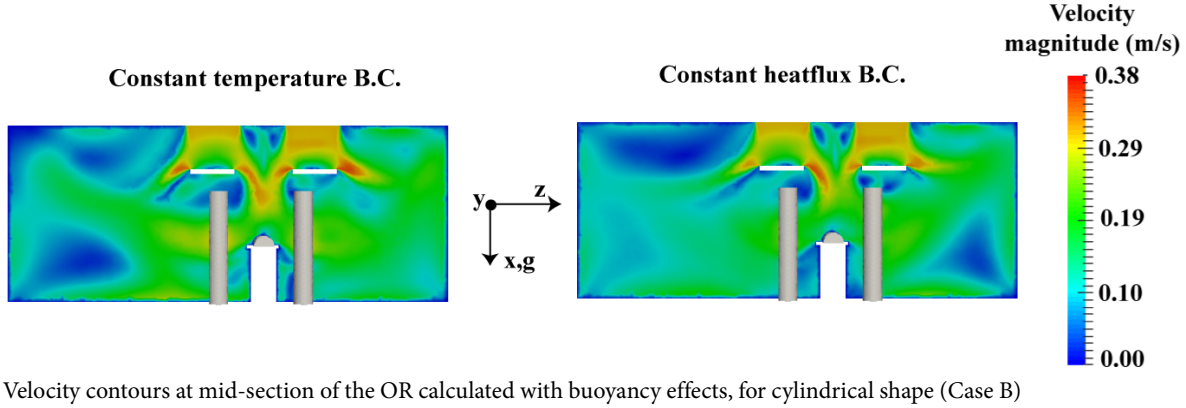

Fig. 8 Velocity contours at mid-section of the OR calculated with buoyancy effects, for cylindrical shape (Case B)

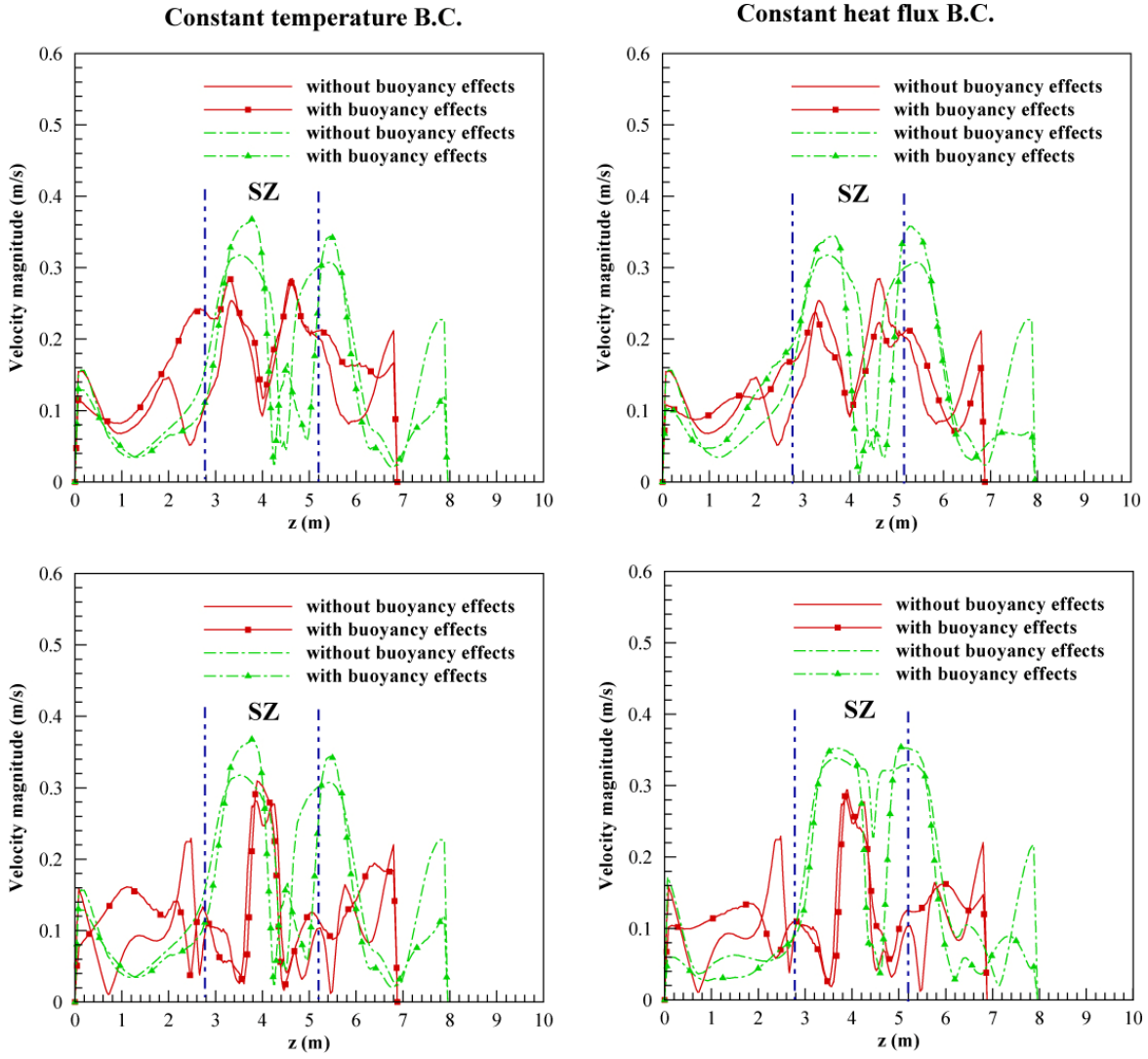

Fig. 9 Velocity profiles at two sections of the OR (green and red lines of Figure 7), at plane heights of 1.1 m (top) and 1.7 m (bottom) for cylindrical shape (Case B), obtained imposing temperature (left) and heat flux (right) boundary conditions on the cylinders (refer to Tables 4 and 5 for the values)

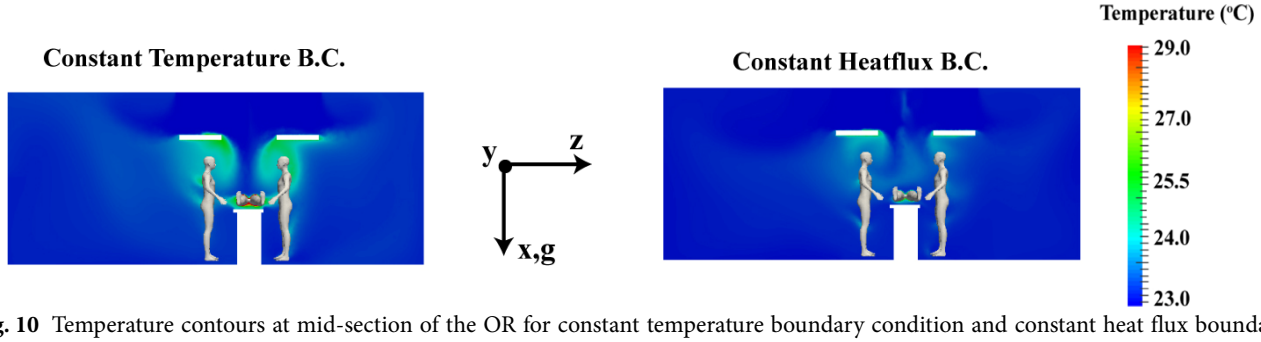

Fig. 10 Temperature contours at mid-section of the OR for constant temperature boundary condition and constant heat flux boundary condition with buoyancy effects, for human body shape (Case A)

air temperature between 26 and 26.3 °C. If buoyancy effects are considered, there is a proper air mixing, creating lower temperature regions (24–25°C). Moreover, at a plane height of 1.7 m (Figure 11 bottom) where the head and shoulder of the medical staff are located (red line), the temperature values are larger with respect to plane height of 1.1 m, due to the lower air velocity recirculation regions, as described before.

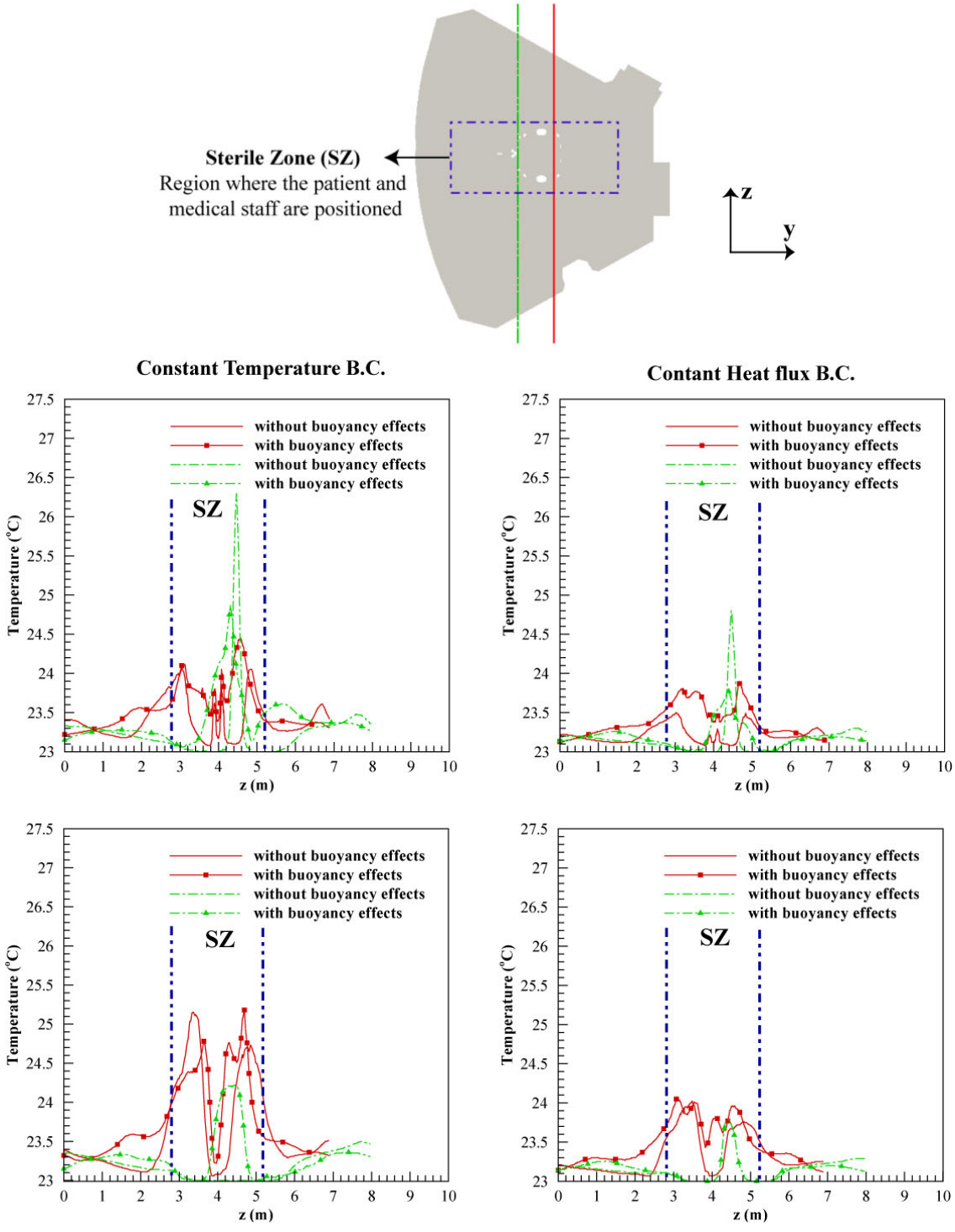

Fig. 11 Temperature profiles at two sections of the OR (green and red lines), at plane heights of 1.1 m (top) and 1.7 m (bottom) for human body shape (Case A), obtained imposing temperature (left) and heat flux (right) boundary conditions on the human bodies (refer to Tables 4 and 5 for the values)

Substituting real human geometries with cylinders (Case B), a slight difference can be observed on temperature distribution inside the OR, as shown in Figures 12 and 13. In fact, a uniform average temperature of 36 °C is provided as constant temperature boundary condition on the cylinders, with respect to the variable temperature values imposed on the different parts of the real human body shape. In this case, the temperature gradients are lower at the sterile zone, if compared to the real human body shapes and the difference is around 4%–8%.

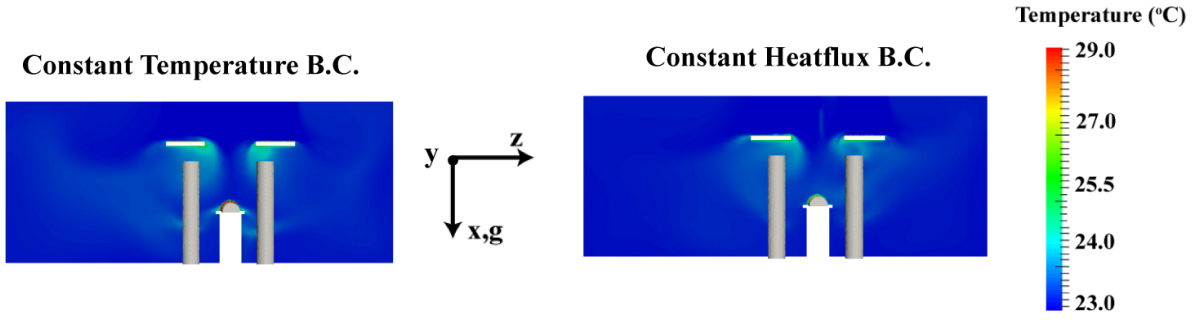

Fig. 12 Temperature contours at mid-section of the OR for constant temperature boundary condition and constant heat flux boundary condition with buoyancy effects for cylindrical shape (Case B)

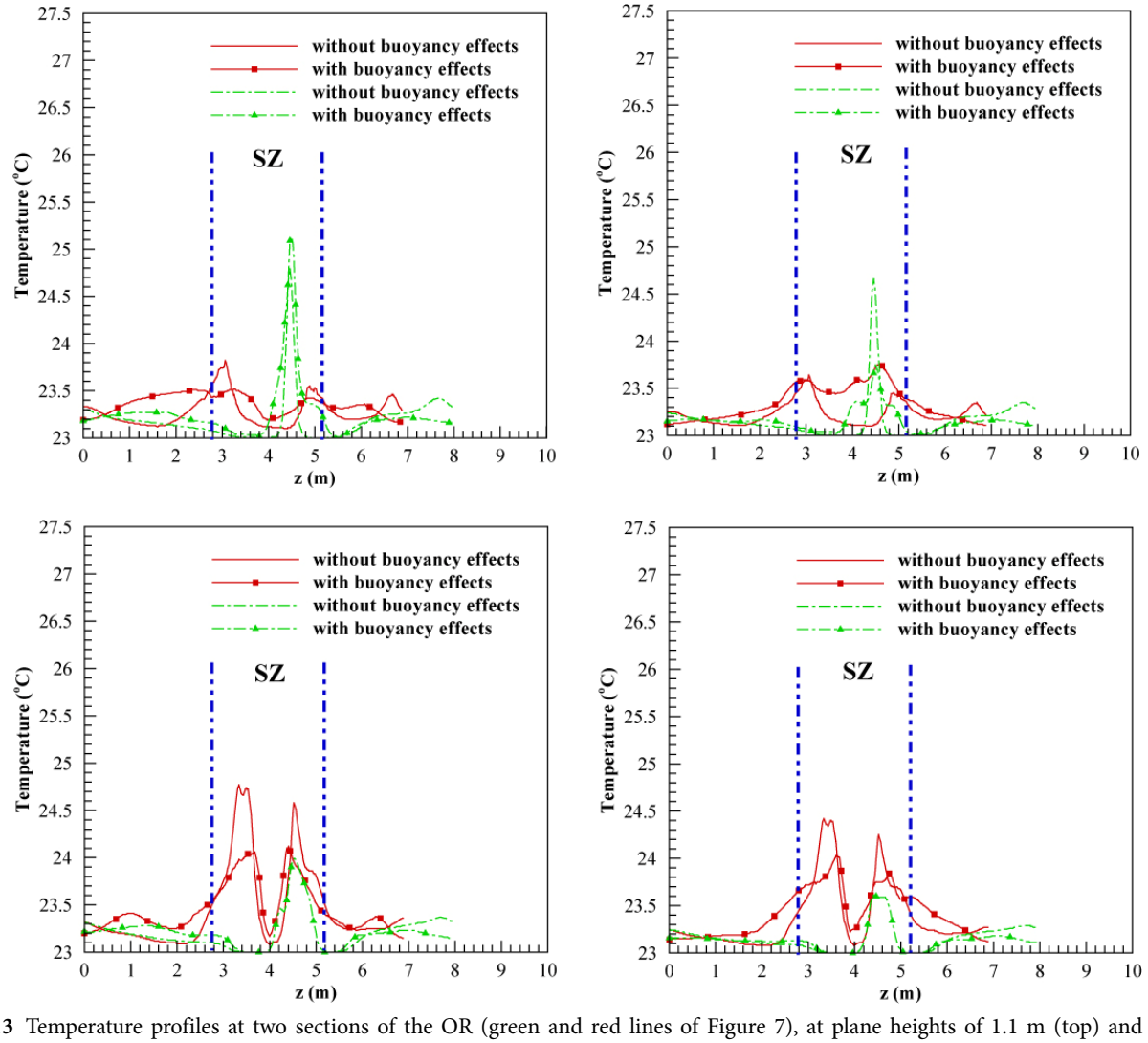

Fig. 13 Temperature profiles at two sections of the OR (green and red lines of Figure 7), at plane heights of 1.1 m (top) and 1.7 m (bottom) for cylindrical shape (Case B), obtained imposing temperature (left) and heat flux (right) boundary conditions on the cylinders (refer to Table 4 and 5 for the values)

3.5 Evaluation of thermal comfort indices: PMV and PPD

The thermal comfort inside the OR is analysed, by means of Predicted Mean Vote (PMV) and Predicted Percentage of Dissatisfied (PPD) indices, which are calculated according to the technical standard ISO 7730. The metabolic energy (M) is considered as 1.20 met, while the clothing insulation (I_{cl}) is assumed as 1 clo.

The temperature values at the real medical staff, patients, surgical lamps and monitor largely affect the air flow, with consequent effects on PMV and PPD indices. Figure 14 shows the PMV index, calculated at the mid-section of the OR with the buoyancy effects, by employing two thermal boundary conditions on the people surfaces, i.e. temperature and heat flux, for human body shape (Case A). Instead, Figure 15 reports the PMV profiles at the same section, at heights of 1.1 m and 1.7 m, for both Case A and Case B. A comparison between thermal indices results with and

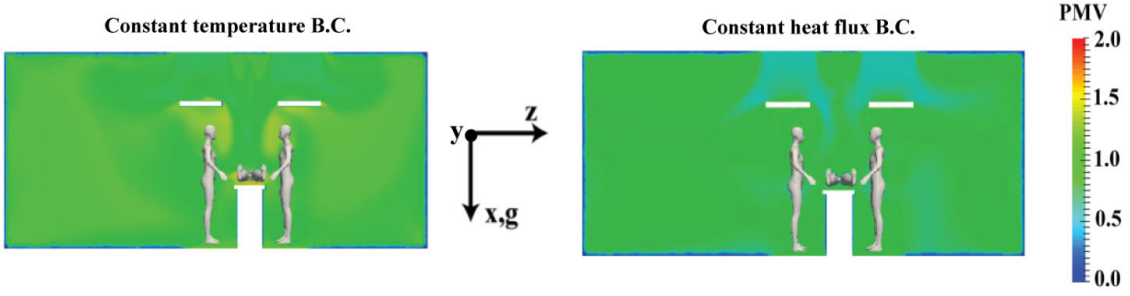

Fig. 14 PMV index field at mid-section of the OR for constant temperature boundary condition (left) and constant heat flux boundary condition (right) with buoyancy effects for real human body (Case A)

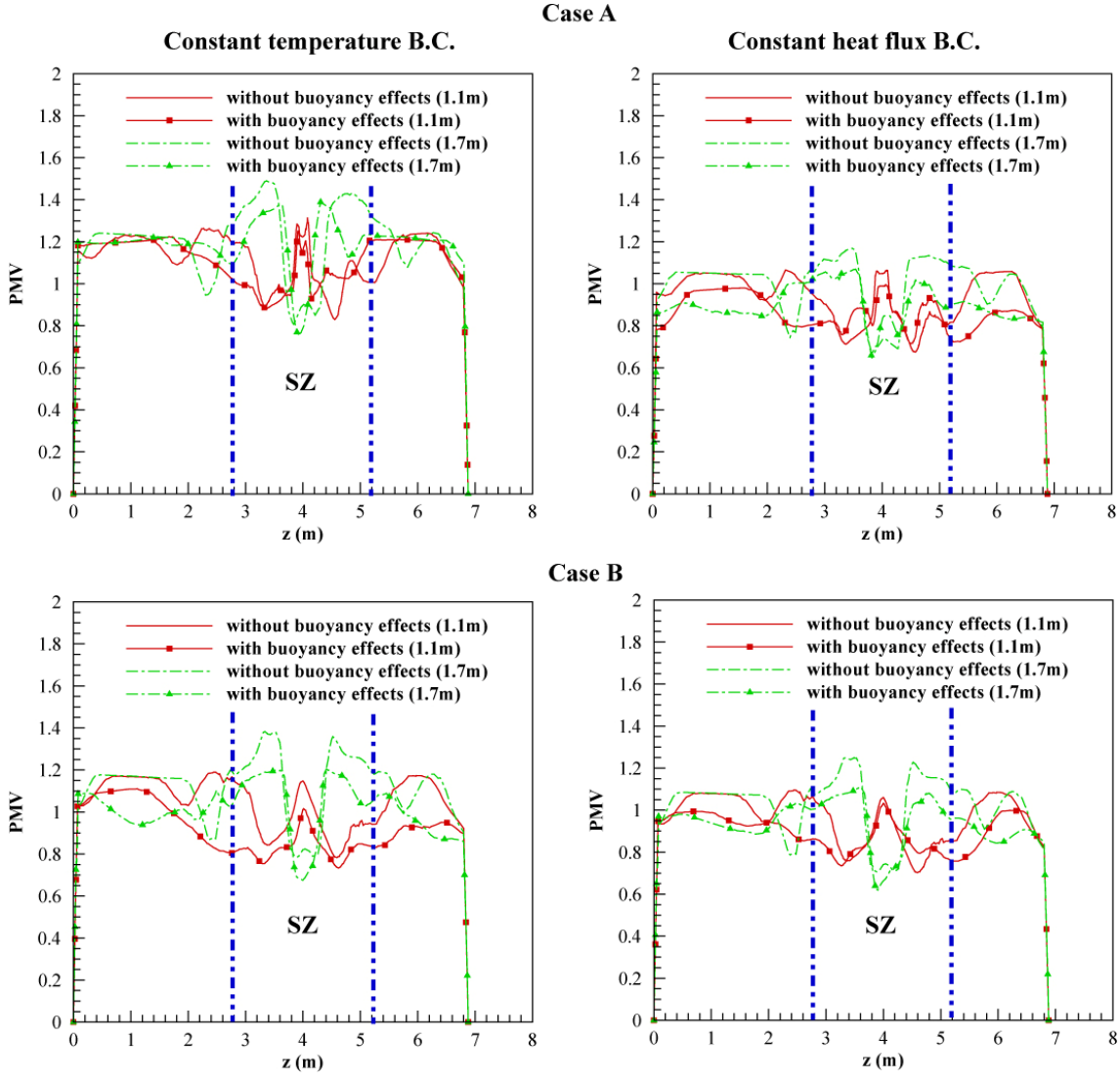

Fig. 15 PMV index profiles at two heights, 1.1m and 1.7m, at the mid-section of the OR for Case A (top) and Case B (bottom) for constant temperature boundary condition (left) and constant heat flux boundary condition (right)

without buoyancy effects are also shown in Figure 15. From the analysis of Figures 14 and 15 with buoyancy effects, it is possible to notice that for constant temperature boundary condition, the air entering the room encounters the surgical lamps and monitors, with consequent local increase of velocity and non-uniformity of airflow. This increase in velocity has a significant effect on the thermal comfort in the OR. In particular, near the head of the medical staff, i.e. at 1.7 m, a PMV value between 0.7 and 1.5 is calculated (Figure 14 left and Figure 15 left—Case A), which corresponds to PPD index of 22%–50%, leading to a thermal sensation of slightly warm condition. Instead, at the plane height of 1.1 m, as discussed in the previous sections, the air velocity near the patient is around 0.05–0.08 m/s and there are more uniform airflow and temperature distribution (23 °C). Therefore, the PMV index is between 0.9 and 1.3, with a consequent PPD index of 22-40%, slightly lower than those calculated at 1.7 m.

In presence of constant heat flux boundary condition on medical staff and patient with buoyancy effects (Figure 14 right and Figure 15 right—Case A), PMV index is between 0.6 and 1.1 with a PPD of 12%–30%, at a height of 1.7 m. Instead, at a height of 1.1 m, PMV index is between 0.7 and 1.0, with a PPD of 12%–26%. Therefore, the employment of heat flux boundary conditions allows to calculate better comfort conditions, with respect to the constant temperature boundary condition. In addition, the presence of buoyancy effects has an effect on the thermal comfort indices when compared to the cases without buoyancy effects as corroborated in Figure 15.

The values of PMV and PPD indices outside the sterile zone are smaller than those calculated in the sterile area, and are in perfect agreement with the values suggested by the technical standard ISO 7730. This is due to the difference of velocity and temperature fields between the different areas of the room, proving that further research in this field is useful to optimize the design of OR and obtain the optimal comfort conditions for medical staff and patient.

A comparative study in terms of thermal comfort has been carried out considering medical staff and patient modelled with real human bodies (Case A) and cylinders (Case B). Figure 15 bottom reports PMV index for Case B, calculated at mid-section, at heights of 1.1 m and 1.7 m, with and without the buoyancy effects, while Figure 16 reports the PPD index field. The indices calculated for both case A and case B are similar. However, in the case of cylindrical geometries, the PMV and PPD indices have a maximum difference of about 10% with respect to Case A.

4 Conclusions

The authors have developed a three-dimensional numerical model able to reproduce the thermo-fluid dynamic conditions inside a real operating room (OR), provided with a unidirectional airflow system, and to calculate the thermal comfort indices. An experimental campaign has been carried out on site, in order to acquire data to be used both as boundary conditions and for validation purposes. An analysis of the measurement uncertainties has been also carried out. After validation, the model has been used to analyse the effects of the following conditions on the airflow, temperature field and comfort indices: (i) reproduction of medical staff and patient with a human body shape (Case A) and with a cylindrical shape (Case B); (ii) presence of buoyancy forces; (iii) employment of two different boundary conditions on people surfaces, i.e. temperature and heat flux boundary condition.

The main conclusions obtained from the present combined numerical-experimental study are:

1) The air velocity and temperature numerical values are in good agreement with the experimental data, within the measurement uncertainty intervals.
2) The air velocity values calculated at the sterile zone can be up to 20% larger if temperature boundary condition is imposed on medical staff and patient, instead of heat flux, proving the importance of the choice of thermal boundary conditions on the results.
3) The buoyancy forces influence the air flow pathlines and velocities, and a difference up to 15% can be appreciated in the sterile zone with respect to the results obtained in absence of buoyancy forces.

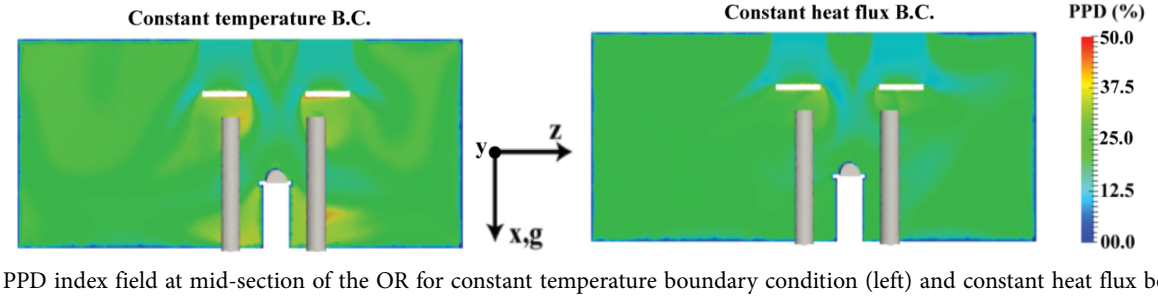

Fig. 16 PPD index field at mid-section of the OR for constant temperature boundary condition (left) and constant heat flux boundary condition (right) with buoyancy effects (bottom) for cylinders (Case B)

4) At the sterile zone, due to the low velocity recirculation regions below the surgical lights, the thermal gradients are larger if temperature boundary condition is imposed instead of heat flux, and the head of the medical staff experiences an air temperature around 24.5 °C.
5) The medical staff can feel slight warm thermal conditions, based on the PMV and PPD values calculated at 1.7 m, equal to 0.6–1.1 and 12%–30%, respectively, due to the difference of velocity and temperature fields between the different areas of the room, proving that further research is useful to optimize the design of OR and obtain the optimal comfort conditions. It should be pointed out that these values depend on many factors, such as the position of people, lamps, monitors and equipment and, therefore, can be optimized.
6) The numerical results obtained for medical staff and patient modelled with real human shapes and cylindrical shapes have a maximum difference around 15%; therefore, for a more detailed analysis, a realistic human shape should be considered, while cylinders can be used as approximation, in order to save computing resources.

The present combined numerical-experimental approach is useful for assessing the effects of thermal boundary conditions on medical staff and patient, such as the employment of realistic and cylindrical geometries, on the flow and thermal fields in the OR. Moreover, based on the predicted thermal comfort conditions, it would be possible to improve the design of HVAC systems and ORs, such as their operation, obtaining optimal comfort conditions.

Acknowledgements

The authors gratefully acknowledge the ASL of Caserta for giving the possibility to use the OR for the experimental tests.

References

Ahl T, Dalen N, Jörbeck H, Hobom J (1995). Air contamination during hip and knee arthroplasties: Horizontal laminar flow randomized vs. conventional ventilation. *Acta Orthopaedica Scandinavica*, 66: 17–20.

Al-Waked R (2010). Effect of ventilation strategies on infection control inside operating theatres. *Engineering Applications of Computational Fluid Mechanics*, 4: 1–16.

ASHRAE (2017). ANSI/ASHRAE/Standard-170, Ventilation of HEALTHCARE Facilities. Atlanta: American Society of Heating, Refrigerating and Air-Conditioning Engineers.

Arpino F, Massarotti N, Mauro A, Vanoli L (2011). Metrological analysis of the measurement system for a micro-cogenerative SOFC module. *International Journal of Hydrogen Energy*, 36: 10228–10234.

Arpino F, Dell'Isola M, Maugeri D, Massarotti N, Mauro A (2013). A new model for the analysis of operating conditions of micro-cogenerative SOFC units. *International Journal of Hydrogen Energy*, 38: 336–344.

Arpino F, Cortellessa G, Mauro A (2015). Transient thermal analysis of natural convection in porous and partially porous cavities. *Numerical Heat Transfer, Part A: Applications*, 67: 605–631.

Arpino F, Carotenuto A, Ciccolella M, Cortellessa G, Massarotti N, et al. (2016). Transient natural convection in partially porous vertical annuli. *International Journal of Heat and Technology*, 34: S512–S518.

ASME (2009). Standard for Verification and Validation in Computational Fluid Dynamics and Heat Transfer. The American Society of Mechanical Engineers.

Balocco C, Petrone G, Cammarata G, Vitali P, Albertini R, Pasquarella C (2014). Indoor air quality in a real operating theatre under effective use conditions. *Journal of Biomedical Science and Engineering*, 7: 866–883.

Balocco C, Petrone G, Cammarata G, Vitali P, Albertini R, et al. (2015). Experimental and numerical investigation on airflow and climate in a real operating theatre under effective use conditions. *International Journal of Ventilation*, 13: 351–368.

Brohus H, Hylding M, Kamper S, Vachek U (2008). Infuence of disturbance on bacteria level in an operating room. In: Proceedings of the 11th International Conference on Indoor Air Quality and Climate, Copenhagen, Denmark.

Chow TT, Yang X (2003). Performance of ventilation system in a non-standard operating room. *Building and Environment*, 38: 1401–1411.

Chow T, Yang X (2004). Ventilation performance in operating theatres against airborne infection: review of research activities and practical guidance. *Journal of Hospital Infection*, 56: 85–92.

Chow TT, Lin Z, Bai W (2006). The integrated effect of medical lamp position and diffuser discharge velocity on ultra-clean ventilation performance in an operating theatre. *Indoor and Built Environment*, 15: 315–331.

Clark RP, Toy N (1975). Natural convection around the human head. *The Journal of Physiology*, 244: 283–293.

Diao C, Zhu L, Wang H (2003). Cooling and rewarming for brain ischemia or injury: theoretical analysis. *Annals of Biomedical Engineering*, 31: 346–353.

DIN-1946-4 (2016). Ventilation and air conditioning—Part 4: Ventilation in buildings and rooms of health care. DIN Standards Committee Heating and Ventilation Technology and their Safety.

Fiala D, Lomas KJ, Stohrer M (1999). A computer model of human thermoregulation for a wide range of environmental conditions: the passive system. Journal of Applied Physiology, 87:1957-1972.

Fojtlín M, Psikuta A, Toma R, Fišer J, Jícha M (2018). Determination of car seat contact area for personalised thermal sensation modelling. *PLoS ONE,* 13(12): e0208599.

Friberg B, Friberg S (2005). Aerobiology in the operating room and its implications for working standards. *Proceedings of the Institution of Mechanical Engineers, Part H: Journal of Engineering in Medicine*, 219: 153–160.

Ginalski MK, Nowak AJ, Wrobel LC (2007). A combined study of heat and mass transfer in an infant incubator with an overhead screen. *Medical Engineering & Physics*, 29: 531–541.

Gordon RG, Roemer RB, Horvath SM (1976). A mathematical model of the human temperature regulatory system—transient cold exposure response. *IEEE Transactions on Biomedical Engineering*, BME-23: 434–444.

Ho SH, Rosario L, Rahman MM (2009). Three-dimensional analysis for hospital operating room thermal comfort and contaminant removal. *Applied Thermal Engineering*, 29: 2080–2092.

ISO14644-1 (2015). Cleanrooms and associated controlled environements—Part 1: Classification of air cleanliness by particle concentration.

ISO14644-2 (2015). Cleanrooms and associated controlled environments—Part 2: Monitoring to provide evidence of cleanroom performance related to air cleanliness by particle concentration.

ISO-7730 (2006). Ergonomics of the thermal environment—Analytical determination and interpetration of thermal comfort using calculation of the PMV and PPD indices and local thermal comfort criteria.

Jeter SM, Stevenson TC (2013). Comparison of CFD simulation of hospital operating room air distribution with experimental PIV results. *ASHRAE Transactions*, 119: 63–74.

Kameel R, Khalil E (2003). Simulation of flow, heat transfer and relative humidity characteristics in air-conditioned surgical operating theatres. In: Proceedings of 41st Aerospace Science Meeting and Exhibit, Reno, NV, USA.

Knobben BAS, van Horn JR, van der Mei HC, Busscher HJ (2006). Evaluation of measures to decrease intra-operative bacterial contamination in orthopaedic implant surgery. *Journal of Hospital Infection*, 62: 174–180.

Laszczyk JE, Nowak AJ (2016). Computational modelling of neonate's brain cooling. *International Journal of Numerical Methods for Heat & Fluid Flow*, 26: 571–590.

Lewis HE, Foster AR, Mullan BJ, Cox RN, Clark RP (1969). Aerodynamics of the human microenvironment. *The Lancet*, 293: 1273–1277.

Liu J, Wang H, Wen W (2009). Numerical simulation on a horizontal airflow for airborne particles control in hospital operating room. *Building and Environment*, 44: 2284–2289.

Loomans M, van Houdt W, Lemaire AD, Hensen JKN (2008). Performance assessment of an operating theatre design using CFD simulation and tracer gas measurements. *Indoor and Built Environment*, 17: 299–312.

Massarotti N, Ciccolella M, Cortellessa G, Mauro A (2016). New benchmark solutions for transient natural convection in partially porous annuli. *International Journal of Numerical Methods for Heat & Fluid Flow*, 26: 1187–1225.

Massarotti N, Mauro A, Sainas D, Marinetti S, Rossetti A (2019). A novel procedure for validation of flow simulations in operating theaters. *Science and Technology for the Built Environment*, 25: 629–642.

McNeill J, Zhai ZJ, Hertzberg J (2012). Field measurements of thermal conditions during surgical procedures for the development of CFD boundary conditions. *ASHRAE Transactions*, 118: 596–609.

McNeill J, Hertzberg J, Zhai Z (2013). Experimental investigation of operating room air distribution in a full-scale laboratory chamber using particle image velocimetry and flow visualization. *Journal of Flow Control, Measurement & Visualization*, 1: 24–32.

Memarzadeh F, Manning A (2002). Comparison of operating room ventilation systems in the protection of the surgical site, *ASHRAE Transaction*, 108: 3–15.

Méndez C, San José JF, Villafruela JM, Castro F (2008). Optimization of a hospital room by means of CFD for more efficient ventilation. *Energy and Buildings*, 40: 849–854.

Mitchell D, Wyndham CH, Vermeulen AJ, Hodgson T, Atkins AR, et al. (1969). Radiant and convective heat transfer of nude men in dry air. *Journal of Applied Physiology*, 26: 111–118.

Najjaran A (2012). Determining natural convection heat transfer coefficient of human body. *Transaction of Control and Mechanical Systems*, 1: 362–369.

Nithiarasu P, Liu C-B, Massarotti N (2007). Laminar and turbulent flow calculations through a model human upper airway using unstructured meshes. *Communications in Numerical Methods in Engineering*, 23: 1057–1069.

Nobile M, Navone P, Orzella A, Colciago R, Auxilia F, Calori G (2015). Developing a model for analysis the extra costs associated with surgical site infections (SSIs): an orthopaedic and traumatological study run by the Gaetano Pini Orthopaedic Institute. *Antimicrobial Resistance and Infection Control*, 4: P68.

Ostrowski Z, Rojczyk M, Szczygieł I, Łaszczyk J, Nowak AJ (2016). Dry heat loses of newborn baby in infant care bed: use of a thermal manikin. *Journal of Physics: Conference Series*, 745: 032087.

Ostrowski Z, Rojczyk M (2018). Natural convection heat transfer coefficient for newborn baby. *Heat and Mass Transfer*, 54: 2395–2403.

Pourshaghaghy A, Omidvari M (2012). Examination of thermal comfort in a hospital using PMV–PPD model. *Applied Ergonomics*, 43: 1089–1095.

Romano F, Marocco L, Gustén J, Joppolo CM (2015). Numerical and experimental analysis of airborne particles control in an operating theater. *Building and Environment*, 89: 369–379.

Sadrizadeh S, Tammelin A, Ekolind P, Holmberg S (2014). Influence of staff number and internal constellation on surgical site infection in an operating room. *Particuology*, 13: 42–51.

Sadrizadeh S, Pantelic J, Sherman M, Clark J, Abouali O (2018). Airborne particle dispersion to an operating room environment during sliding and hinged door opening. *Journal of Infection and Public Health*, 11: 631–635.

Shih T-H, Liou WW, Shabbir A, Yang Z, Zhu J (1995). A new k-ε eddy viscosity model for high Reynolds number turbulent flows. *Computational Fluids*, 24: 227–238.

Topp C, Nielsen PV, Sørensen DN (2002). Application of computer simulated persons in indoor environmental modeling. *ASHRAE Transactions*, 108(2): 1084–1089.

Topp C, Hesselholt P, Trier MR, Nielsen PV (2003). Influence of geometry of thermal manikins on room airflow. In: Proceedings of Healthy Buildings.

van Gaever R, Jacobs VA, Diltoer M, Peeters L, Vanlanduit S (2014). Thermal comfort of the surgical staff in the operating room. *Building and Environment*, 81: 37–41.

van Leeuwen GMJ, Hand JW, Lagendijk JJW, Azzopardi DV, Edwards AD (2000). Numerical modeling of temperature distributions within the neonatal head. *Pediatric Research*, 48: 351–356.

Verheyen J, Theys N, Allonsius L, Descamps F (2011). Thermal comfort of patients: Objective and subjective measurements in patient rooms of a Belgian healthcare facility. *Building and Environment*, 46: 1195–1204.

Wilkins CK, McGaffin N (1994). Measuring computer equipment loads in office buildings. *ASHRAE Journal*, 36(8): 21–24.

Zoon WAC, van der Heijden MGM, Loomans MGLC, Hensen JLM (2010). On the applicability of the laminar flow index when selecting surgical lighting. *Building and Environment*, 45: 1976–1983.

Zoon WAC, Loomans MGLC, Hensen JLM (2011). Testing the effectiveness of operating room ventilation with regard to removal of airborne bacteria. *Building and Environment*, 46: 2570–2577.

Zukowska D, Melikov A, Popiolek Z (2007). Thermal plume above a simulated sitting person with different complexity of body geometry. In: Proceedings of the 10th International Conference on Air Distribution in Rooms (Roomvent 2007), Helsinki, Finland.